Fermi National Accelerator Laboratory

FERMILAB-Pub-99/004-A

Multiple-streaming and the Probability Distribution of Density in Redshift Space

Lam Hui

Fermi National Accelerator Laboratory
P.O. Box 500, Batavia, Illinois 60510

Lev Kofman

McLennan Physical Labs
60 St. George Street, Toronto, Ontario M5S 3H8, Canada

Sergei F. Shandarin

University of Kansas
Lawrence, Kansas 66045

January 1999

Submitted to *Astrophysical Journal*

Operated by Universities Research Association Inc. under Contract No. DE-AC02-76CH03000 with the United States Department of Energy

Disclaimer

Distribution

Copyright Notification

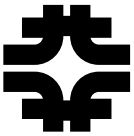

Fermi National Accelerator Laboratory

FERMILAB–PUB–99/004-A
CITA-99-1
astro-ph/9909104
January 13, 1999

Multiple-streaming and the Probability Distribution of Density in Redshift Space

Lam Hui*
NASA/Fermilab Astrophysics Center
Fermi National Accelerator Laboratory, Batavia, IL 60510

Lev Kofman†
CITA, McLennan Physical Labs
60 St George Street, Toronto ON M5S 3H8, Canada

Sergei F. Shandarin‡
Department of Physics and Astronomy
University of Kansas, Lawrence, KS 66045

*e-mail: lhui@fnal.gov

†e-mail: kofman@cita.utoronto.ca

‡e-mail: sergei@kusmos.phsx.ukans.edu

Operated by Universities Research Association Inc. under contract with the United States Department of Energy

ABSTRACT

We examine several aspects of redshift distortions by expressing the redshift-space density in terms of the eigenvalues and orientation of the local Lagrangian deformation tensor. We explore the importance of multiple-streaming using the Zel'dovich approximation (ZA), and compute the average number of streams in both real and redshift-space. It is found that multiple-streaming can be significant in redshift-space but negligible in real-space, even at moderate values of the linear fluctuation amplitude ($\sigma_\ell \lesssim 1$). Moreover, unlike their real-space counter-parts, redshift-space multiple-streams can flow past each other with minimal interactions. Such nonlinear redshift-space effects, which are physically distinct from the fingers-of-God due to small-scale virialized motions, might in part explain the well-known departure of redshift distortions from the classic linear prediction by Kaiser (1987), even at relatively large scales where the corresponding density field in real-space is well described by linear perturbation theory. We also compute using the ZA the probability distribution function (PDF) of density, as well as S_3, in real and redshift-space, and compare it with the PDF measured from N-body simulations. The role of caustics in defining the character of the high density tail is examined. It is found that (non-Lagrangian) smoothing, due to both finite resolution or discreteness and small-scale velocity dispersions, is very effective in erasing caustic structures, unless the initial power spectrum is sufficiently truncated.

Subject headings: cosmology: theory — gravitation — large-scale structure of universe

1. Introduction

The distortion of the density field in redshift-space by peculiar motion is an old subject (see e.g. Sargent & Turner 1977; Bean et al. 1983; Davis & Peebles 1983; Kaiser 1987; Hamilton 1992). It is commonly held that on small scales, virialized motion causes the stretching of structures along the line of sight, creating what is often called the fingers-of-God, while on large scales, coherent infall into high density regions causes compression, thereby making structures appear more wall-like in the tangential directions than they are in real-space. The reader is referred to Hamilton (1996) for a comprehensive review.

It has also been recognized for some time, however, that the classic linear prediction by Kaiser (1987) overpredicts the compression, even at relatively large scales where the corresponding density field in real-space is quite linear ($\sigma_\ell \lesssim 1$). Conversely, the dilution effect embodied by the fingers-of-God appears to extend to rather large scales. (See e.g. Suto & Suginohara 1991; Fisher et al. 1993;

Gramann et al. 1993; Brainerd et al. 1996; Bromley et al. 1997.) We will refer to this phenomenon as translinear redshift distortions.

This effect has often been discussed in the context of attempts to measure β ($\Omega_m^{0.6}/b$, where b is the bias) using the ratio of the real-space to redshift-space two-point function or the quadrupole-to-monopole ratio of the redshift-space power spectrum (see e.g. Cole et al. 1994). It is found, both from observations, as well as from N-body simulations, that the linear theory predictions for these ratios fail even at very large scales, where perturbation theory is known to work well in real-space. In general, one finds that the amount of line-of-sight squashing of the redshift-space two-point function is overpredicted by the linear perturbative formulae. The large uncertainties in published values of β are at least in part due to our poor understanding of this effect (see Table 1 of Hamilton 1996).

A related phenomenon has also been observed in studies of one-point statistics of the density field in redshift-space, albeit in a slightly more subtle form. Hivon et al. (1995) computed the leading perturbative contribution to S_3 and S_4 in redshift-space. They observed that the agreement on large scales between the predicted values and the measured values from N-body simulations is not as good as it is in the case of real-space. Only at very small σ_ℓ (the linear fluctuation amplitude in real-space; in other words, very large smoothing scales) did they obtain rough agreements. In fact, above some moderate σ_ℓ (~ 0.2), the value of S_N in redshift-space generally lies below that in real-space, suggesting an effect that resembles the fingers-of-God.

Recently, Taylor & Hamilton (1996) and Fisher & Nusser (1996) (see also Hatton & Cole 1997 for detailed comparisons with simulations) revisited this issue by computing the quadrupole-to-monopole ratio of the redshift-space power spectrum using the Zel'dovich approximation (Zel'dovich 1970; henceforth as ZA). Both pairs of authors were able to obtain accurate predictions for the shape of the quadrupole-to-monopole ratio on translinear scales. In particular, they demonstrated analytically that the departure from the linear prediction could take place at relatively large scales, and they interpreted the success of the ZA in accounting for this effect as an indication that the failure of the linear prediction on translinear scales have more to do with coherent infall rather than virialized motion.

It is our aim here to continue this line of investigation of nonlinear effects in redshift distortions, but we will focus our attention on one-point statistics. Following earlier work by McGill (1990), we explore the role of caustics and multiple-streaming in redshift-space. It was pointed out by McGill (1990), who used one-dimensional Zel'dovich dynamics, that redshift-space caustics could form even when the real-space density field is only mildly nonlinear. We will quantify this by computing the average number of streams in both real and redshift-space using the ZA. As will be shown, at $\sigma_\ell \sim 1$, the degree of multiple-streaming could be significant in redshift-space but negligible in real-space. This is covered in §3.2.

The above finding indicates that the real to redshift-space mapping enhances the level of nonlin-

earity. An interesting feature of multiple-streaming in redshift-space is that, unlike their real-space counterparts, redshift-space multiple streams to a first approximation can flow freely past each other (at least before real-space caustics actually form), because they arise from physically distinct regions in real-space. This might provide an interesting explanation for why the famous Kaiser formulae overpredicts the amount of redshift-space compression along the line of sight, even at moderate σ_ℓ's. Redshift-space multiple-streams could then provide a mechanism for counteracting the linear compression. The free-crossing of redshift-streams in the intermediate regime is not unlike the familiar phenomenon of the thickening of the ZA pancake. In this sense, the ZA, which can be viewed as a local approximation where interaction is ignored (see Shandarin & Zel'dovich 1989 for a review; see also Kofman & Pogosyan 1995; Hui & Bertschinger 1996), is well-suited for studying this phenomenon.

The formalism for computing the average number of streams was in fact originally developed to calculate the full one-point probability distribution function (PDF hereafter) of density. Our work here is a natural extension of earlier work by Kofman et al. (1994) who computed the PDF in real-space using the ZA. We will also use the same methodology to compute the PDF as well as the skewness S_3 in both real and redshift-space in the small σ_ℓ limit. The formalism is laid out in §2, the computational method is explained in §3.1, and the results of the PDF and S_3 calculation are discussed in §3.3 and 3.4.

We particularly focus our attention on the high density regime of the PDF. Catastrophe theory tells us that caustics generally induce a ρ^{-3} tail, which, however, is not observed in N-body simulations with CDM-type (Cold-Dark-Matter) power spectra, either in real or redshift-space. In fact, an intriguing property of the PDF in CDM models is that it is well-fit by a single parameter lognormal distribution (in both real and redshift-space), where the caustic-tail is absent (for real space, see e.g. Kofman et al. 1994; Bernardeau & Kofman 1995). We explore the reason for it in §4, and conclude that smoothing in redshift-space (or in real-space), due to both finite resolution or discreteness and small-scale velocity dispersions, plays an important role in erasing the caustic-feature in the PDF [§]. To understand properly the behavior of the PDF then requires a non-local calculation, which is beyond the scope of this paper. We briefly discuss possible lines of attack in §5.

2. Formalism

For the purpose of this article, we denote by ρ and ρ_z the densities in real (or Eulerian) and redshift space respectively, normalized by the mean density (i.e. $\langle\rho\rangle = \langle\rho_z\rangle = 1$). The evolution of ρ is determined by the mapping from Lagrangian to Eulerian space, according to mass conservation:

[§]Smearing of caustics in the HDM model due to the thermal velocities was considered by Zel'dovich & Shandarin (1982) and Kotok & Shandarin (1987).

$$\rho = \left| \det^{-1} \left[\frac{\partial x^i}{\partial q^j} \right] \right| , \tag{1}$$

where x^i and q^j are the Eulerian and Lagrangian coordinates. They are related by the displacement D^j

$$\mathbf{x} = \mathbf{q} + \mathbf{D} . \tag{2}$$

Similarly, the evolution of the redshift-space density is determined by the mapping from Eulerian to redshift-space:

$$\mathbf{s} = \mathbf{x} + \frac{1+z}{H} (\mathbf{v} \cdot \mathbf{e}) \mathbf{e} , \tag{3}$$

where $\mathbf{s}$ is the redshift-space coordinate, z is the mean redshift of interest, H is the Hubble parameter at redshift z, $\mathbf{v}$ is the peculiar velocity and $\mathbf{e}$ is the unit vector along the line of sight.

The redshift-space density ρ_z is then given by ¶

$$\rho_z = \left| \det^{-1} \left[\frac{\partial s^i}{\partial q^j} \right] \right| = \rho \left| \det^{-1} \left[\frac{\partial s^i}{\partial x^j} \right] \right| = \rho \left| 1 + \frac{1+z}{H} \frac{\partial \mathbf{v}}{\partial x^i} \cdot \mathbf{e} e^i \right|^{-1} , \tag{4}$$

where eq. (1) has been used for the second equality. We have used the remote-observer approximation for the third equality, in other words, setting the term $\partial \mathbf{e} / \partial x^i = 0$. This is equivalent to assuming the directional unit vector does not change appreciably for a small displacement in the transverse direction. In addition, an interesting matrix identity has also been used: $\det[\delta_{ij} + A_i B_j] = 1 + \mathbf{A} \cdot \mathbf{B}$, where $\mathbf{A}$ and $\mathbf{B}$ are arbitrary vectors.

Let us now introduce the Zel'dovich approximation (ZA) to model the dynamics.

The ZA consists of assuming $\mathbf{D} \propto D_+$ where D_+ is the linear time-dependent growth factor. Growing mode (in other words, irrotational) initial condition then implies

$$\mathbf{D} = -D_+ \nabla_{\mathbf{q}} \psi , \tag{5}$$

where ψ is the displacement potential and $\nabla_{\mathbf{q}}$ in component form is $\partial / \partial q^i$.

The peculiar velocity is then simply $\mathbf{v} = \dot{\mathbf{D}}$, where the derivative is with respect to conformal time for a fixed $\mathbf{q}$.

Putting the above into eq. (4), we arrive at the following expression for ρ_z

$$\rho_z = \left| \det{}^{-1} \mathbf{X} \ (1 + f X^{-1}_{ik} D^k{}_j e^i e^j)^{-1} \right| , \tag{6}$$

where

$$X_{ij} = \delta_{ij} + D_{ij} \quad , \quad D_{ij} = -D_+ \frac{\partial^2 \psi}{\partial q^i \partial q^j} , \tag{7}$$

¶This is the single-stream redshift-space density. See discussion at the end of the section.

and $f \equiv \dot{D}a/(D\dot{a}) \sim \Omega_m^{0.6}$ (Peebles 1980),[||] with a being the scale factor and Ω_m being the fraction of critical density in matter.

Therefore, for a given Ω_m, ρ_z is uniquely determined by the line-of-sight unit vector e^i and the displacement matrix D_{ij}. The probability distribution of ρ_z is then dictated by the probability distributions of the later two quantities.

For random orientations of the line-of-sight, the distribution of e^i is given by

$$P(e^i)de^i = \sin\theta \, d\theta d\phi \,, \tag{8}$$

where $[e^1, e^2, e^3] = [\sin\theta\cos\phi, \sin\theta\sin\phi, \cos\theta]$.

For Gaussian random initial conditions, the probability distribution, in Lagrangian space, of the displacement matrix D_{ij} can be computed exactly. One can always go to a frame in which D_{ij} is diagonal, keeping in mind that the line-of-sight is randomly oriented with respect to the eigenvectors of this matrix. All we need then is the probability distribution of its eigenvalues. We will denote this probability distribution in Lagrangian space by $P(\lambda_j)d\lambda_j$, where λ_j's ($j = 1, 2, 3$) are the eigenvalues of $-D_{ij}$, $\lambda_1 \geq \lambda_2 \geq \lambda_3$.

Accordingly, eq. (6) can be rewritten as

$$\rho_z = |(1-\lambda_1)(1-\lambda_2)(1-\lambda_3)(1 - f\sum_i \frac{\lambda_i}{(1-\lambda_i)}(e^i)^2)|^{-1} \tag{9}$$

or further as

$$\begin{aligned} \rho_z = \quad & |\,(1+f)(1-\lambda_1)(1-\lambda_2)(1-\lambda_3) \\ & -f[(1-\lambda_2)(1-\lambda_3)e_1^2 + (1-\lambda_1)(1-\lambda_3)e_2^2 + (1-\lambda_1)(1-\lambda_2)e_3^2]\,|^{-1} \end{aligned} \tag{10}$$

Thus, the density in redshift-space can ultimately be expressed in terms of the eigenvalues and orientation of the local Lagrangian deformation tensor. The statistical properties of ρ_z can then be inferred from the well-known statistics of the deformation tensor. Eqs. (9), (11) represents a redshift-space generalization of the familiar Zel'dovich formulae for the density in real-space. Just like the Zel'dovich result in real space, it sheds light on the main features of the local structures in redshift space. The first three factors in Eq. (9) obviously arise from the mapping from the Lagrangian to Eulerian (or real) space and the last factor comes from that from real to redshift-space. The latter mapping strongly depends on the orientation of the deformation tensor with respect to the line of sight **e**.

[||] A more accurate expression for f can be found in Lahav et al. 1991 and Carroll et al. 1992, but we will adopt $f \sim \Omega_m^{0.6}$, which is a very good approximation at $z = 0$.

In Fig. 1, we show an example of the density evolution of of a fluid element, with the eigenvalues today ($D_+ = 1$) of $\lambda_1 = 1, \lambda_2 = 0.5$ and $\lambda_3 = -0.5$. Two cases are considered: when the line of sight is aligned with the axis of fastest collapse (λ_1) (short dashed line), and when the line of sight is aligned with the eigenvector associated with λ_3 (long dashed line). The evolution of the real-space density is shown as a solid line. The real-space density formally diverges at $D_+ = 1$ because of caustic-formation. The redshift-space density tends to become nonlinear even earlier. In particular, this redshift-space amplification works most efficiently if the axis of the fastest collapse is aligned with the line of sight. What we have here can be interpreted as a nonlinear manifestation of the linear effect noticed by Kaiser (1987). Note how the redshift-space density decreases after (redshift-) caustic formation (at $D_+ = 0.5$, for the short dashed line). This corresponds to the free-crossing of redshift-space multiple-streams, which counteracts the Kaiser compression of structures along the line of sight.

It is also important to emphasize that eq. (9) only gives us a local picture of the density distribution. As in the familiar case of the ZA in real-space, our local Lagrangian treatment suggests an anisotropic structure, except that the structure is preferentially transverse to the line of sight. However, it should be cautioned that the above equations tell us nothing about the global distribution of these local structures, whether they are aligned in a filament or a sheet is actually determined by the correlation function of shear (see Bond et al. 1996). Moreover, small-scale velocity dispersions are likely to at least smear out the caustics, which we will come back to later. The only situation in which we can say something about the global distribution of structures using our local Lagrangian description is for a truncated initial power spectrum, in other words with a displacement field that is smoothed on large scales in Lagrangian space, similar to what is done in the truncated Zel'dovich approximation (Kofman et al. 1992; Coles et al. 1993).

Let us now define two different probability distribution functions (PDF) of density, following the treatment of Kofman et al. (1994).

The Lagrangian PDF of (redshift-space) density is:

$$P_{\rm L}(\rho_z) = \int \delta_D(\rho_z - \rho_z{}')P(\lambda_j)d\lambda_j P(e^i)de^i\,, \tag{11}$$

where δ_D is the Dirac delta function, $\rho_z{}'$ in its argument is a function of λ_j and e^i as expressed in eq. (9), $P(e^i)de^i$ is given by eq. (8), and $P(\lambda_j)d\lambda_j$ is the probability that a given Lagrangian element has the set of eigenvalues λ_j's falling in the prescribed ranges. In other words, $P_{\rm L}(\rho_z)d\rho_z$ tells us the fraction of the Lagrangian volume that has the redshift-space density $\rho_z \pm d\rho_z/2$.

To obtain the redshift-space PDF of the (redshift-space) density, two effects need to be taken into account. The redshift-space PDF is supposed to tell us the fraction of the redshift space volume that has the redshift-space density within a particular range, say $\rho_z \pm d\rho_z/2$. The first effect arises from the fact that the Lagrangian and redshift-space PDFs differ by a multiplicative volume factor:

a given Lagrangian volume corresponds to a different redshift-space volume. This factor is none other than ρ_z itself. In other words, the redshift-space PDF should be equal to the Lagrangian PDF divided by ρ_z.

If there were no multiple-streaming, this would be the whole story. The second effect that has to be taken into account is illustrated schematically in Fig. 2. Multiple-streaming is said to occur in places where the mapping from $\mathbf{q}$ to $\mathbf{s}$ is no longer one-to-one.

The expression for ρ_z in eq. (4) is defined for every Lagrangian coordinate $\mathbf{q}$. In other words, it is a single-stream redshift-space density. In regions where multiple-streaming occurs, the actual redshift-space density, at a particular $\mathbf{s}$ say, should be a sum of ρ_z's over all $\mathbf{q}$'s that map onto the same $\mathbf{s}$. Such a non-local calculation is beyond the scope of this paper. Instead, following Kofman et al. (1994), we assume the fraction of the total redshift-space volume that is occupied by these multiple-stream-regions is not large (i.e. mildly nonlinear regime). However, there are inevitably some such regions. A renormalizing factor N_s is then needed when computing the redshift-space PDF:

$$P_{\rm z}(\rho_z) = {N_s}^{-1} {\rho_z}^{-1} P_{\rm L}(\rho_z)\,, \tag{12}$$

where $P_{\rm L}$ is given in eq. (11) and

$$N_s = \int_0^\infty {\rho_z}^{-1} P_{\rm L}(\rho_z) d\rho_z\,. \tag{13}$$

The factor of ${\rho_z}^{-1}$ takes care of the first effect mentioned above: it is the ratio of redshift-space volume to Lagrangian-space volume. However, since ρ_z is the single-stream redshift-space density, an overcounting of the total redshift-space volume over the total Lagrangian-space volume occurs. The true ratio of the two should be unity. N_s gives the ratio of the total *single-stream* redshift-space volume to the total Lagrangian-space volume (the latter is also equal to the true total redshift-space volume with no overcounting), which is in general larger than 1 because of multiple-streaming (or, in other words, overcounting). This quantity provides the correct renormalizing factor for $P_{\rm z}$.

An additional bonus of the above formalism is that we have a quantitative measure of the degree of multiple-streaming in N_s. It tells us the average number of streams at an arbitrary point in redshift-space. Fig. 2 provides a nice illustration of how N_s should be interpreted. Suppose V^T is the total true (no overcounting) volume in redshift-space (i.e. the "volume" shown on the y-axis). Suppose further that V^1 is the part of V^T that is in single-stream regions, and V^3 is the part that is in triple-stream regions i.e. $V^T = V^1 + V^3$. Recall that N_s is the ratio of the total *single-stream* redshift-space volume to the total true redshift-space volume, which means $N_s = (V^1 + 3V^3)/V^T = P(1) + 3P(3)$, where $P(1)$ and $P(3)$ are the probabilities that a given region is in single-stream and triple-stream regimes respectively. Hence, N_s is exactly what one would refer to as the average number of streams at a point in redshift-space. Obviously, the argument extends to higher (but always odd) number of streams.

Note furthermore that while eq. (12) gives only an approximate redshift-space PDF in the limit of little multiple-streaming (N_s close to 1), eq. (13) is an exact expression for the average number of streams, at least within the framework of the ZA. This should be kept in mind in the discussion of the next section.

Lastly, note that the above expressions (eq. [9], [11], [12], [13]) reduce to their real-space counterparts in the limit $f = 0$, in other words, when the real to redshift-space mapping is trivial.

3. The Average Number of Streams and the PDF: Method and Results

3.1. Method

The quantities we are interested in are $P_{\rm z}(\rho_z)$ and N_s in eq. (12) and (13). Both of them require performing the integral in eq. (11). Kofman et al. (1994) succeeded in reducing the analog of this integral in real-space (i.e. setting $f = 0$ in eq. [9]) to a one-dimensional integral which has to be done numerically. Redshift-space distortions introduce extra complications. We will instead perform the integral in eq. (11) numerically right from the beginning. The delta function restriction $\delta_D[\rho_z - \rho_z{}'(\lambda_j, e_i)]$ is most easily dealt with using Monte Carlo techniques (see Reisenegger & Miralda-Escude 1995 for a similar calculation in the context of the PDF of the optical depth rather than the density in redshift-space). In other words, we generate realizations of λ_j's and e^i's, and identify combinations of them which satisfy the delta function restriction. The directional unit vector e^i is easily handled because it is randomly distributed over the 2-sphere, with the probability distribution given by eq. (8). On the other hand, the probability distribution for the λ_j's is somewhat more complicated.

The probability distribution of the eigenvalues of the displacement matrix D_{ij}, for a Gaussian random field, was first calculated by Doroshkevich (1970). We adopt a form for this distribution which is better suited for the Monte Carlo computation outlined above (following Bertschinger & Jain 1994; see also Reisenegger & Miralda-Escude 1995). Let $-\lambda_j$'s be the eigenvalues of the displacement matrix D_{ij}, and let Δ, γ and α be variables defined through λ_j's as follows

$$[\lambda_1, \lambda_2, \lambda_3] = \frac{\Delta}{2}\cos\gamma[1,1,1] + \frac{\Delta}{\sqrt{5}}\sin\gamma[\cos(\frac{\alpha+2\pi}{3}), \cos(\frac{\alpha-2\pi}{3}), \cos(\frac{\alpha}{3})]\,, \qquad (14)$$

where the Δ ranges from 0 to infinity, and both γ and α are between 0 and π. The above ranges enforce the ordering $\lambda_1 \le \lambda_2 \le \lambda_3$. It can be shown that for any given combination of λ_i's in this order, there corresponds a unique set of Δ, γ and α.

The probability distribution of λ_j's is given by (Bertschinger & Jain 1994):

$$P(\lambda_j)d\lambda_j = \left[\frac{1}{16}\left(\frac{3}{2\sigma_\ell}\right)^6 \Delta^4 \exp\left(-\frac{\Delta^2}{2}\left[\frac{3}{2\sigma_l}\right]^2\right) d\Delta^2\right]\left[\frac{8}{3\pi}\sin^4\gamma d\gamma\right]\left[\frac{1}{2}\sin\alpha d\alpha\right]\,. \qquad (15)$$

where σ_ℓ is the root-mean-squared (rms) amplitude of the linear real-space density fluctuation.

A nice feature of the set of variables Δ, γ and α is that their joint probability distribution factorizes. Δ^2 is distributed like a gamma-deviate. $8\sin^4\gamma/(3\pi)d\gamma$ can be integrated exactly to give $d\eta/2$ where $\eta = 1-2\gamma/\pi+4\sin2\gamma/(3\pi)-\sin4\gamma/(6\pi)$, so that η is distributed uniformly between -1 and 1. Lastly, $\cos\alpha$ is also uniformly distributed between -1 and 1. Standard numerical methods exist for generating variables distributed in the above manner (see Press et al. 1992).

Note that the only free parameters in the above calculation are σ_ℓ and Ω_m, or more precisely, f. The former controls the distribution of λ_j's through eq. (15), while the latter determines the degree of redshift-space distortion (eq. [6] or [9]).

3.2. The Average Number of (Lagrangian) Streams

Fig. 3 shows the result of the calculation outlined above for N_s, the average number of Lagrangian streams, defined in eq. (13). This is shown as a function of σ_ℓ (eq. 15), the rms amplitude of the linear real-space density fluctuation, for three different values of Ω_m. The $\Omega_m = 0$ case corresponds to the average number of streams in real-space.**

Several points should be noted. First, redshift-space distortion, or peculiar motion, has the effect of increasing the amount of multiple-streaming over that in real-space. Second, a larger Ω_m means more redshift-space distortion, hence a higher average number of streams.

At $\sigma_\ell = 1$, the average number of streams in real-space is very close to 1.0, while the average number of streams in redshift-space is 1.1 and 1.2 for $\Omega_m = 0.3$ and $\Omega_m = 1$ respectively. This means multiple-streaming can be insignificant in real-space, but going on in earnest in redshift-space.†† In other words, even at relatively small σ_ℓ, when the real-space density field is quite linear, redshift-space distortion introduces inherently non-perturbative effects through multiple-streaming.

The above result perhaps explains the success of perturbation theory, which is by nature a single-stream theory, in estimating various statistics of the density field in real-space, at $\sigma_\ell \lesssim 1$ (Many references should be cited here, see Juszkiewicz & Bouchet 1995 and Bernardeau 1996 for short reviews. See also Scoccimarro & Frieman 1996 and Scoccimarro 1997 for loop corrections which can be important at large enough σ_ℓ.). The same does not appear to be true for statistics of the redshift-space density field, however. For instance, it is well-known that the linear-theory redshift

---

**Fig. 1 of Kofman et al. (1994) contains an error for the real-space average number of streams. For the perturbative result in real-space, see also Munshi, Sahni & Starobinsky (1994).

††1.2 might not seem too different from 1.0. However, it should be kept in mind this means, at any given point in redshift-space, one finds on the average 1.2 streams. In other words, the total single-stream redshift-volume is 20% higher than the total true redshift-volume.

distortion factor deduced by Kaiser (1987) fails to describe the quadrupole-to-monopole ratio of the redshift-space power spectrum even at very large scales (see Hatton & Cole 1997 and references therein for a recent discussion). This failure is an indication of the importance of non-perturbative effects such as those due to multiple-streaming in redshift-space.

The fact that multiple-streaming in real-space is less severe than multiple-streaming in redshift-space has another interesting implication. Recall the Lagrangian to real-space to redshift-space mapping: $\mathbf{q} \rightarrow \mathbf{x} \rightarrow \mathbf{s}$. The multiple-(Lagrangian)-streaming in redshift-space arises not so much from the $\mathbf{q} \rightarrow \mathbf{x}$ mapping (otherwise, the average number of Lagrangian streams in real-space would not be so close to 1 for, say, $\sigma_\ell = 1$), but rather from the $\mathbf{x} \rightarrow \mathbf{s}$ mapping.

This is interesting because the multiple-streams at a given $\mathbf{s}$ then mostly come from distinct places in real space i.e. they do not interact strongly, unlike the case of multiple-(Lagrangian)-streams at the same $\mathbf{x}$. One well-known failure of the Zel'dovich Approximation is that it does not account for the gravitational interaction between different Lagrangian streams around a real-space caustic i.e. the different streams (unphysically) freely go past each other at a Zel'dovich pancake. Around a redshift-space caustic, however, the multiple streams can (approximately) free-stream past each other because they are not located at the same real-space location. This might provide a mechanism for partially canceling the line-of-sight compression of structures pointed out by Kaiser (1987).

3.3. The PDF of Redshift-space and Real-Space Density

We compute the PDF of redshift-space density according to eq. (12) for $\Omega_m = 1$ and $\Omega_m = 0$, and for 2 different σ_ℓ's: the result is shown in Fig. 4. The $\Omega_m = 0$ curves correspond also to the PDFs of the real-space density. We have chosen σ_ℓ's small enough so that the average number of streams is close to 1 (see Fig. 3). This is to ensure the validity of the approximation involved in eq. (12).

It can be seen that peculiar motion has the effect of making the PDF look more nonlinear in redshift-space than it is in real-space. This should be expected based on the Kaiser (Kaiser 1987) effect alone: large scale coherent infall into initial density enhancements (in real-space) shifts such regions further out into the high-density tail of the PDF, while at the same time creating lower-density voids thereby making the PDF peak at lower densities.

At higher σ_ℓ's, translinear distortions, or redshift-space multiple-streaming, would start to cancel the Kaiser compression, and begin to cause dilution around the initial density enhancements. At still higher σ_ℓ's, a qualitatively different dilution effect, the finger-of-God, kicks in due to the formation of virialized clusters. This happens after multiple-streaming becomes important in real-space. Unfortunately, the PDF as expressed in (9) is incapable of taking multiple-streaming (in

either redshift or real-space) properly into account, as we have explained in §2. Nonetheless, we will attempt to probe into the regime of multiple-streaming by considering the effect of caustics on the high ρ_z tail of the PDF in §4.

How good is the ZA-predicted PDF as a description of the true PDF? We show in Fig. 5 a comparison of the ZA PDF versus the PDF measured from an $\Omega_m = 1$ CDM simulation, for two different output times, smoothed at the same comoving scale. The linear CDM power spectrum has $\Gamma = 0.25$, and the box size is 100 h^{-1}Mpc, simulated on a 128^3 grid. The reader is referred to the Hydra consortium (`http://coho.astro.uwo.ca/pub/data.html`; see also Couchman et al. 1995) for further details of the simulation. The one free parameter we have to fix for the ZA prediction is the linear fluctuation amplitude σ_ℓ. It can be seen that, as expected, σ_ℓ is always smaller than the fluctuation amplitude of the evolved-and-smoothed density field, which we call $\sigma_{\rm nl}$. We also show lognormal distributions which reproduce the evolved fluctuation amplitude of the simulation outputs. In other words,

$$P_{\rm logn.}(\rho_z) = \frac{1}{\sqrt{2\pi}\sigma_{\rm eff}\rho_z} e^{-\frac{1}{2\sigma_{\rm eff}^2}(\ln\rho_z + \frac{1}{2}\sigma_{\rm eff})^2}, \tag{16}$$

where $\sigma_{\rm eff}$ is chosen to equal $\sqrt{\ln(1+\sigma_{\rm nl}^2)}$. It is impressive how well it fits the N-body data out to large ρ_z's. The same phenomenon has been observed in real-space for a similar cosmological model (Kofman et al. 1994). The error-bars are estimated by dividing the box into 4 different subsamples, and computing the dispersion. It should be emphasized that we have purposefully chosen outputs, with suitable smoothing, that are only mildly nonlinear, so that the average number of Lagrangian streams is very close to 1, making eq. (12) a good approximation.

The overall agreement between the ZA PDF and the N-body data is decent at these low values of σ_ℓ. However, the ZA PDF tends to overpredict the probability of high ρ_z. It is in fact well-known that the ZA PDF has a long tail of $P(\rho_z) \propto 1/\rho_z^3$, due to the presence of caustics. This is true in both real and redshift-space. It implies that, unfortunately, σ_ℓ has to be left as a free parameter in the above comparison because the ZA PDF does not yield a well-defined $\sigma_{\rm nl}$. We will revisit this issue in §4.

3.4. S_3 in Redshift-space and Real-space

The methodology outlined in §3.1 can be easily adopted to compute other one-point statistics, such as S_3:

$$S_3 = \frac{\langle(\rho_z - 1)^3\rangle}{\langle(\rho_z - 1)^2\rangle^2} \tag{17}$$

As in the case of $\sigma_{\rm nl}$, because of the caustic-induced tail of the ZA PDF, S_3 is, strictly speaking, undefined except in the limit of vanishing σ_ℓ. The finite number of realizations used in our Monte

Carlo method provides a natural regularization by truncating at some high ρ_z's, thereby giving a finite S_3. As one decreases the input parameter σ_ℓ in the Monte Carlo integration, the output S_3 converges eventually to the correct ZA predicted value for infinitesimal σ_ℓ. Our results are summarized in Table 1 (see also e.g. Bernardeau & Kofman 1995 for the real-space ZA prediction). We find that the rate of convergence for S_4, S_5, etc becomes progressively slower, and so we only give the S_3 values here.

It can be seen that peculiar motion tends to slightly increase S_3 over its real-space value, as the reader might have guessed from the PDFs shown in Fig. 4. This behavior is consistent with what is found by Hivon et el. (1995) in the case of the exact dynamics, in the small σ_ℓ limit. However, as is well-known in the case of real-space, in the perturbative limit, the ZA systematically gives lower S_3 than the exact dynamics.

As emphasized by Hivon et al. (1995), the perturbative prediction breaks down even at relatively small σ_ℓ's (say 0.2), or large smoothing scales, and the actual N-body S_3 is generally *smaller* in redshift-space than in real-space. They attributed it to some kind of finger-of-God effect on large scales, which we view as in part due to multiple-streaming in redshift-space (that is distinct from the familiar small-scale finger-of-God). Unfortunately, the ZA yields a meaningful skewness only in the vanishing σ_ℓ limit, making it difficult to investigate the impact of these effects on S_3.

4. Erasing Caustics ?

Why does the ZA PDF predict a long high-ρ_z tail, and why is it not observed in N-body simulations, at least for CDM-type models? We believe the answer to the latter at least in part has to do with smoothing due to finite resolution or discreteness as well as small-scale velocity dispersions. But let us first briefly review where the high ρ_z tail comes from. The reader is referred to Shandarin & Zel'dovich (1989) for a review. Most of our arguments below apply equally well to real-space caustics.

A caustic is located at a point where ρ_z or $\det^{-1}\partial s_i/\partial q_j$ diverges. As Zel'dovich (1970) originally argued, this is generically due to the vanishing of only one of the eigenvalues of the matrix $\partial s_i/\partial q_j$. Hence, we can focus our attention on the direction that aligns with the eigenvector associated with the vanishing eigenvalue. We will denote the relevant one-dimensional coordinates simply by s and q. The situation is depicted in Fig. 2.

Taylor expanding s as a function of q around $q = q_c$ (corresponding to $s = s_c$ where the caustic is), one can see that to the lowest order, s is a quadratic function of q i.e.

$$s - s_c = \frac{1}{2}\left.\frac{\partial^2 s}{\partial q^2}\right|_{q=q_c} (q - q_c)^2 \tag{18}$$

In other words, ρ_z should fall off as $1/(q-q_c)$ or $1/\sqrt{s-s_c}$, around the caustic. Note that, strictly speaking, ρ_z should be given by the sum over the contribution from each multiple-stream around the caustic (as in the case depicted in Fig. 2), but the singularity due to $1/(q-q_c)$ or $1/\sqrt{s-s_c}$ dominates. Note also that this singular behavior of ρ_z occurs only on one side of the caustic in s-space.

To understand the caustic's influence on the PDF, the crucial point to remember is that one has equal probability of locating at any position in s-space with respect to the location of the caustic. Therefore, $P(s)ds \propto P(\rho_z)d\rho_z$, with $P(s)$ independent of s, from which the $P(\rho_z) \propto 1/\rho_z^3$ behavior follows. The premise is that asymptotically high ρ_z's occur only around caustics.

Why is the caustic-induced feature of the PDF then not observed?

We believe the answer lies in final (as opposed to initial or Lagrangian) smoothing. There are two sources of final smoothing: one due to finite resolution or the discrete nature of the simulations (or observations), and the other due to smearing by small-scale velocity dispersions. Two conditions have to be met for the caustic-induced high ρ_z tail to survive these kinds of inevitable smoothing in s-space.

First, it is important that the scale of the caustic in s-space, $\Delta s_{\rm caustic}$, is larger than the smoothing scale, $\Delta s_{\rm smooth}$, where the smoothing scale can be taken to be whichever is dominant of the two kinds of smoothing mentioned above $\Delta s_{\rm smooth} = \max(\Delta s_{\rm res.}, \sigma_v(1+z)/H)$. The smoothing scale $\Delta s_{\rm res.}$ is associated with the finite final resolution, and σ_v is the velocity dispersion along the line of sight.

The scale of the caustic in s-space is related to its counterpart in q-space by eq. (18):

$$\Delta s_{\rm caustic} = \frac{1}{2}\left|\frac{\partial^2 s}{\partial q^2}\right|_{q_c} \Delta q^2_{\rm caustic}\,, \tag{19}$$

where $\Delta q_{\rm caustic}$ is the scale of the caustic in q-space. A good definition for $\Delta q_{\rm caustic}$ is given by the magnitude of $q-q_c$ such that the next higher order term ignored in eq. (18) becomes significant. In other words, $\Delta q_{\rm caustic} \sim [\partial^3 s/\partial q^3]^{-1}[\partial^2 s/\partial q^2]$. One can use even higher order terms for its definition, but it would not affect our arguments below.

Let us then express the first condition for the survival of the caustic-induced feature as

$$\Delta s_{\rm smooth} < \frac{1}{2}\left|\frac{\partial^2 s}{\partial q^2}\right|_{q_c} \Delta q^2_{\rm caustic}\,. \tag{20}$$

The second condition has to do with the density profile of a smoothed caustic. Assume that the first condition above is met, the smoothed profile of the caustic would be given by $\rho_z(s) = f(s)/\sqrt{|\partial^2 s/\partial q^2|_{q_c}\Delta s_{\rm smooth}}$ where $f(s)$ is some dimensionless profile which, at its peak, is equal to $O(1)$. This is a very generic prediction quite independent of the form or origin of the smoothing.

This means the smoothed caustic peaks at $\rho_{z\max} \sim 1/\sqrt{|\partial^2 s/\partial q^2|_{q_c} \Delta s_{\rm smooth}}$. Now, if one would like such a smoothed caustic to contribute to the high ρ_z tail, it is important that $\rho_{z\max} \gg 1$. Hence, the second condition for the survival of the caustic-induced feature in the PDF is:

$$\left|\frac{\partial^2 s}{\partial q^2}\right|_{q_c} \ll \frac{1}{\Delta s_{\rm smooth}} \tag{21}$$

The two conditions in eq. (20) and (21) together imply the necessary requirement that

$$\frac{\Delta s_{\rm smooth}}{\Delta q_{\rm caustic}} \ll 1\,. \tag{22}$$

Therefore, the only remaining question is what the typical $\Delta q_{\rm caustic}$ should be. This can be estimated using the definition suggested before: that $\Delta q_{\rm caustic}$ is given by $[\partial^3 s/\partial q^3]^{-1}\ [\partial^2 s/\partial q^2]$ evaluated at the caustic. One can calculate exactly what the average value of this ratio should be, for Gaussian initial conditions, imposing the constraint that the first derivative vanishes. All one needs is the joint probability distribution of all the derivatives up to the third one *at a single point*. However, there is no need to do any calculation. The only relevant scale in this problem is the *initial* smoothing scale of the density field (or the displacement field) in q-space, let us call it $\Delta q_{\rm smooth}$. Therefore $\Delta q_{\rm caustic} \sim \Delta q_{\rm smooth}$.

For CDM-type power spectra, the initial smoothing scale $\Delta q_{\rm smooth}$ is of the order of a few grid-spacings (unless the initial power spectrum is deliberately smoothed or truncated), while the final smoothing scale $\Delta s_{\rm smooth}$ is at least also a few grid-spacings (and probably even larger due to small-scale velocity dispersions). This implies the condition in eq. (22) is never met, hence explaining why the theoretical caustic-induced tail of the PDF is not observed, at least in CDM simulations. In other words, to understand the high-ρ_z behavior of the PDF properly, both multiple-streaming and smoothing have to be properly taken into account. This also points to a weakness of the calculation presented in §2. Because final smoothing in s-space is not taken into account in the formalism, effects like what is discussed above are missed. We hope to pursue improvement of the calculation in this direction in the future.

5. Discussion

Using the Zel'dovich approximation, we find that peculiar motion significantly raises the degree of multiple-streaming. We quantify this by computing the average number of Lagrangian-streams in both real and redshift-space. As is shown in Fig. 3, multiple-streaming can be insignificant in real-space, but non-negligible in redshift-space, even at moderate values of σ_ℓ. This implies that most of the multiple-streaming in redshift-space arises from the $\mathbf{x} \to \mathbf{s}$ mapping (real or Eulerian to redshift-space), rather than from the $\mathbf{q} \to \mathbf{x}$ mapping (Lagrangian to Eulerian space).

That the level of nonlinearity is amplified by the real to redshift-space mapping implies non-perturbative effects have to be taken into account in the calculation of redshift distortions, even on scales where the real-space density field is relatively linear. An interesting feature of redshift-space multiple-streaming is that redshift-space multiple-streams can freely flow past each other, unlike their real-space counterparts. This counteracts the familiar large scale compression of structures along the redshift direction first pointed out by Kaiser (1987), but it is physically distinct from the stretching of structures due to virialized motions on small scales. This might offer an explanation of why, even on relatively large scales, linear theory overpredicts the amount of reshift-space squashing of the two-point function along the line of sight. To make this quantitative, however, requires a detailed calculation, which we will discuss briefly below.

We have computed also using the ZA the probability distribution function (PDF) of density, as well as S_3, in both real and redshift-space. At the largest scales, or small σ_ℓ limit, S_3 does not appear to change significantly from real to redshift-space, consistent with the finding of Hivon et al. (1995). We have compared the ZA PDF with that measured from a CDM N-body simulation (Fig 5). We find that the PDF in redshift-space is well-fit by a lognormal distribution, similar to its counter-part in real-space (Kofman et al. 1994; Bernardeau & Kofman 1995). This suggests the PDF in both real and redshift-space can be described by a single-parameter family of functions ($\sigma_{\rm eff}$ in eq. [16]). This is certainly worth exploring with more N-body simulations and different cosmological models (see Scherrer & Gaztañaga 1998).

The simulation PDF reveals no caustic-induced high ρ_z tail, contrary to the ZA prediction. The same has been observed before in real-space as well (Kofman et al. 1994). We argue in §4 that this is at least in part due to the fact that final smoothing in redshift-space (or real-space) is not taken into account in our formalism. Smoothing naturally arises because of finite resolution or discreteness, as well as due to small-scale velocity dispersions. We give the criterion for the survival of the caustic feature through smoothing in eq. (22): the final-smoothing scale has to be smaller than the Lagrangian-smoothing scale.

In practice, we expect caustics to be efficiently erased by final-smoothing, unless the initial power spectrum is sufficiently smoothed or truncated. This is reminiscent of a related situation in gravitational lensing: that caustic features can only be observed if the source-size is sufficiently small.

As mentioned before, a proper treatment of the statistics of the density field in redshift-space requires tackling the issues of multiple-streaming and final-smoothing. While such a calculation is beyond the scope of the present paper, Taylor & Hamilton (1996) and Fisher & Nusser (1996) have already made significant progress in using the ZA to compute the quadrupole-to-monopole ratio of the redshift-space power spectrum. They use the following expression for the Fourier transform of

the redshift-space density:

$$\tilde{\rho}_z(\mathbf{k}) = \int d^3q e^{-i\mathbf{k}\cdot(\mathbf{q}+\mathbf{D_s})} \tag{23}$$

where $\mathbf{D_s}$ as a function of $\mathbf{q}$ is the displacement from the Lagrangian position $\mathbf{q}$ to the redsfhit-space position $\mathbf{s}$. It comes from the following basic equation for the redshift-space density: $\rho_z(\mathbf{s}) = \int d^3q \delta_D(\mathbf{s}-\mathbf{q}-\mathbf{D_s})$, which implicitly allows for multiple-streaming by automatically summing over density contributions from all possible streams. The key here is that the mapping from real to redshift-space is treated exactly, instead of perturbatively, hence the non-perturbative nature of the redshift-space density field is taken into accout even if the real-space density field is still quite linear. These authors find that the ZA predicts the right-shape for the quadrupole to monopole ratio but underestimates the zero-crossing scale (see also Hatton & Cole 1997). One can take their treatment one step further by using approximations that are closer to the exact dynamics (see e.g. Scoccimarro 1999). Whatever the approach, it appears likely that, because of the prominence of multiple-streaming in redshift-space, a pure perturbative calculation would be inadequate. Non-perturbative effects such as those due to multiple-streaming (or even pre-multiple-streaming) have to be taken into account explicitly.

Lastly, our Lagrangian analysis here still leaves open the question of how the local pancakes or caustics are spatially distributed globally, whether they preferentially lie along filaments or sheets. Calculations have shown that filamentary structures in real-space are preferred for Gaussian initial conditions (e.g. Bond et al. 1996, Yess & Shandarin 1996). It remains to be seen how the redshift-space mapping might alter this picture. Our local calculation, however, does provide a valid description of the global distribution of structures if the initial power spectrum is sufficiently smoothed, as is done in the truncated Zel'dovich approximation.

LH is grateful to Roman Scoccimarro for many useful discussions and help with the simulations. The CDM simulations analyzed in this work were obtained from the data bank of N-body simulations provided by the Hydra consortium (`http://coho.astro.uwo.ca/ pub/data.html`) and produced using the Hydra N-body code (Couchman et al. 1995). LH thanks Dick Bond and the Canadian Institute for Theoretical Astrophysics for hospitality and an excellent working environment. This work was in part supported by the DOE and the NASA grant NAG 5-7092 at Fermilab. SS acknowledges the support of EPSCoR 1998 grant, GRF grant at UK, and thanks the Canadian Institute for Theoretical Astrophysics for hospitality.

References

Bean, A. J., Ellis, R. S., Shanks, T., Efstathiou, G., & Peterson, B. A., 1983, MNRAS **205**, 605
Bernardeau, F., 1996, Proc. of the XXXI Moriond Meeting, Les Arcs, France, astro-ph 9607004
Bernardeau, F. & Kofman, L., 1995, ApJ **443**, 479
Bertschinger, E. & Jain, B., 1994, ApJ **431**, 486

Bond, J. R., Kofman, L., & Pogosyan, D., 1996, Nature **380**, 603

Brainerd, T. G., Bromley, B. C., Warren, M. S., & Zurek, W. H., 1996, ApJ **464**, L103

Bromley, B. C., Warren, M. S., & Zurek, W. H., 1997, ApJ **475**, 414+

Carroll, S. M., Press, W. H., & Turner, E. L., 1992, Ann. Rev. Astr. Ap. **30**, 499

Cole, S., Fisher, K. B., & Weinberg, D. H., 1994, MNRAS **267**, 785+

Coles, P., Melott, A. L., & Shandarin, S. F., 1993, MNRAS **260**, 765

Couchman, H. M. P., Thomas, P. A., & Pearce, F. R., 1995, ApJ **452**, 797+

Davis, M. & Peebles, P. J. E., 1983, ApJ **267**, 465

Doroshkevich, A. G., 1970, Astrofizika **6**, 581

Fisher, K. B., Davis, M., Strauss, M. A., Yahil, A., & Huchra, J. P., 1993, ApJ **402**, 42

Fisher, K. B. & Nusser, A., 1996, MNRAS **279**, L1

Gramann, M., Cen, R., & Bahcall, N. A., 1993, ApJ **419**, 440+

Hamilton, A. J. S., 1992, ApJ **385**, L5

Hamilton, A. J. S., 1996, Proc. of the Ringberg Workshop on Large-Scale Structure, Germany, September, astro-ph 9708102

Hatton, S. J. & Cole, S., 1997

Hivon, E., Bouchet, F. R., Colombi, S., & Juszkiewicz, R., 1995, A&A **298**, 643+

Hui, L. & Bertschinger, E., 1996, ApJ **471**, 1+

Juszkiewicz, R. & Bouchet, F., 1995, Proceedings of the XXX Moriond Meeting. Les Arcs, France. astro-ph 9607004

Kaiser, N., 1987, MNRAS **227**, 1

Kofman, L., Bertschinger, E., Gelb, J. M., Nusser, A., & Dekel, A., 1994, ApJ **420**, 44

Kofman, L. & Pogosyan, D., 1995, ApJ **442**, 30

Kofman, L., Pogosyan, D., Shandarin, S. F., & Melott, A. L., 1992, ApJ **393**, 437

Kotok, E. & Shandarin, S., 1987, Sov. Astr. **31**, 600

Lahav, O., Rees, M. J., Lilje, P. B., & Primack, J. R., 1991, MNRAS **251**, 128

McGill, C., 1990, MNRAS **242**, 428

Munshi, D., Sahni, V. & Starobinsky, A. A. 1994, ApJ, **436**, 517

Peebles, P. J. E., 1980, *The Large Scale Structure of the Universe*, Princeton University Press

Press, W. H., Teukolsky, S. A., Vetterling, W. T., & Flannery, B. P., 1992, *Numerical Recipes*, Cambridge University Press

Reisenegger, A. & Miralda-Escude, J., 1995, ApJ **449**, 476+

Sargent, W. L. W. & Turner, E. L., 1977, ApJ **212**, L3

Scherrer, R. & Gaztañaga, E., 1998, in preparation

Scoccimarro, R., 1997, ApJ **487**, 1+

Scoccimarro, R., 1999, in preparation

Scoccimarro, R. & Frieman, J., 1996, ApJS **105**, 37+

Shandarin, S. F. & Zel'dovich, Y., 1989, Rev. Mod. Phys. **61**, 185

Suto, Y. & Suginohara, T., 1991, ApJ **370**, L15
Taylor, A. N. & Hamilton, A. J. S., 1996, MNRAS **282**, 767
Yess, C. & Shandarin, S., 1996, ApJ **465**, 2
Zel'dovich, Y. B., 1970, **5**, 84
Zel'dovich, Y. B. & Shandarin, S., 1982, Sov. Astr. Lett. **8**, 139

σ_ℓ	Ω_m	S_3
0.01	0	4.0
0.01	0.3	4.1
0.01	1.0	4.2

Table 1: The ZA predicted S_3 in real-space (the $\Omega_m = 0$ case) and redshift-space, for $\sigma_\ell = 0.01$

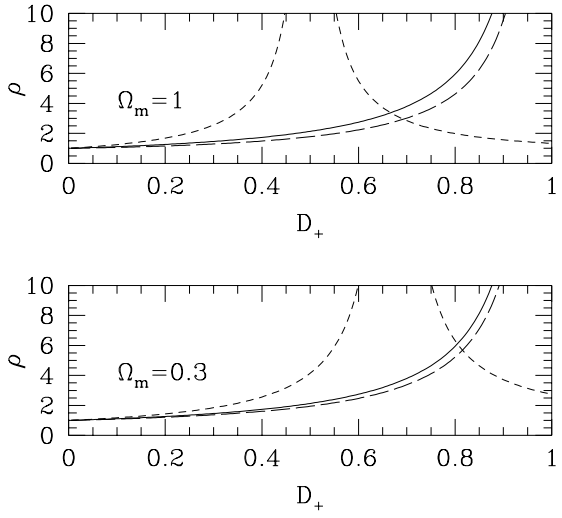

Fig. 1.— The density evolution of a fluid element, as a function of the growth factor D_+. The eigenvalues of the deformation tensor (at $D_+ = 1$) are $\lambda_1 = 1, \lambda_2 = 0.5$ and $\lambda_3 = -0.5$. The solid line shows the evolution of the real-space density. The short and long dashed lines show how the redshift-space density evolves if the line of sight aligns with λ_1 and λ_3 respectively.

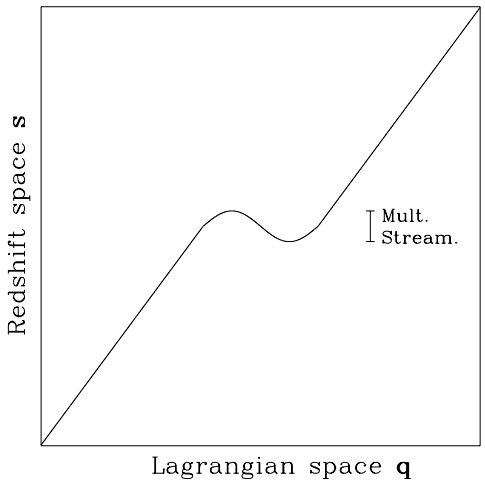

Fig. 2.— A schematic diagram illustrating the mapping from Lagrangian-space to redshift-space. Multiple-streaming occurs in places where the mapping is not one-to-one, in other words, several **q**'s are mapped to the same **s**.

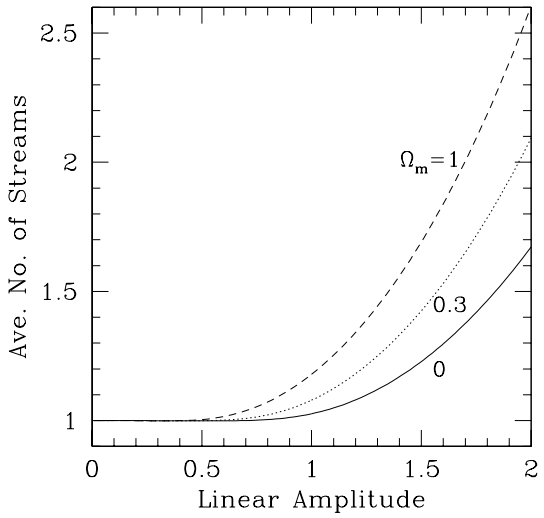

Fig. 3.— The average number of Lagrangian streams in redshift space (N_s) versus the rms amplitude of the linear (real-space) density fluctuation (σ_ℓ), for three different values of Ω_m. The $\Omega_m = 0$ curve gives also the average number of Lagrangian streams in real-space.

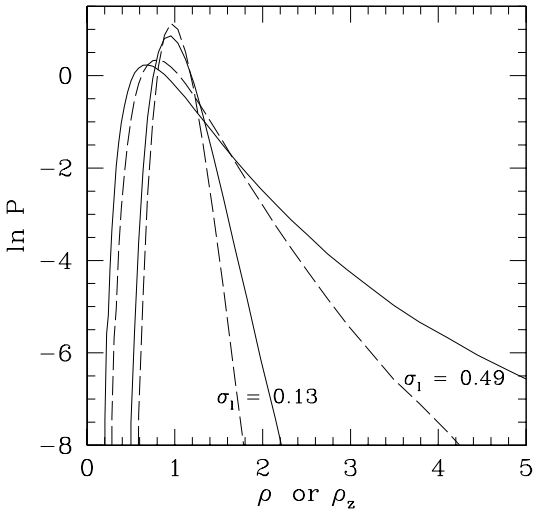

Fig. 4.— The ZA prediction for the PDF of redshift-space (*solid line*) and real-space (*dashed line*) density for two different amplitudes of the linear (real-space) density fluctuation, $\sigma_\ell = 0.13$ and $\sigma_\ell = 0.49$. $\Omega_m = 1$ for the redshift-space curves.

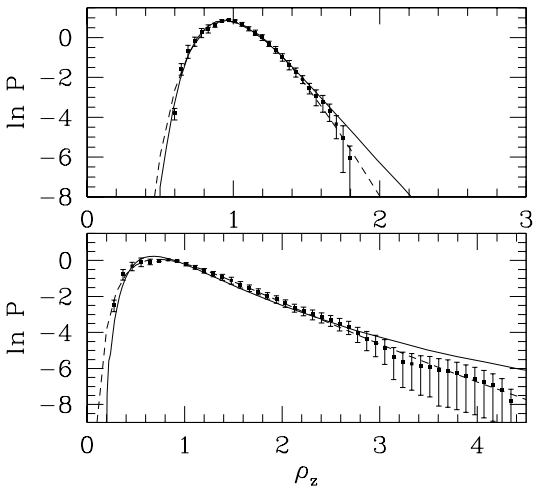

Fig. 5.— Comparison of the ZA-predicted PDFs (*solid lines*) with the measured PDFs (*points with error-bars*) from CDM, $\Omega_m = 1$, N-body simulations. The *dotted lines* represent a lognormal fit to the N-body data. The upper panel is from a simulation output at $a = 0.23$, and the lower panel is from an output at $a = 0.49$, each smoothed with a Gaussian window of $6.25\,\mathrm{h}^{-1}$Mpc. The actual rms amplitudes of the density fluctuation ($\sigma_{\rm nl}$) are 0.34 and 0.49 respectively, while the linear σ_ℓ's used for the ZA-curves are 0.13 and 0.35.